Tailoring Macroscale Response of Mechanical and Heat Transfer Systems by Topology Optimization of Microstructural Details

Joe Alexandersen and Boyan Stefanov Lazarov

Abstract The aim of this book chapter is to demonstrate a methodology for tailoring macroscale response by topology optimizing microstructural details. The microscale and macroscale response are completely coupled by treating the full model. The multiscale finite element method (MsFEM) for high-contrast material parameters is proposed to alleviate the high computational cost associated with solving the discrete systems arising during the topology optimization process. Problems within important engineering areas, heat transfer and linear elasticity, are considered for exemplifying the approach. It is demonstrated that it is important to account for the boundary effects to ensure prescribed behavior of the macrostructure. The obtained microstructures are designed for specific applications, in contrast to more traditional homogenization approaches where the microstructure is designed for specific material properties.

1 Introduction

The focus of this book chapter is on the topology optimization of microstructural details for tailoring the macroscale response of mechanical and heat transfer systems. Topology optimization [7] is an iterative design process which distributes material in a design domain by optimizing a prescribed objective and satisfying a set of constraints. In mechanical and structural engineering applications, the typical objective is to maximize structural stiffness subjected to material constraints, or minimize material volume subjected to stiffness constraints. Over the last decade topology optimization has become one of the preferred design tools in the automotive and aerospace industries. In addition, the method has spread to other disciplines for design of optical crystals and circuits, antennas and fluid mechanics systems [14, 30].

J. Alexandersen (✉) · B.S. Lazarov
Department of Mechanical Engineering, Technical University of Denmark, Kongens Lyngby, Denmark
e-mail: joealex@mek.dtu.dk

B.S. Lazarov
e-mail: bsl@mek.dtu.dk

N.D. Lagaros and M. Papadrakakis (eds.), *Engineering and Applied Sciences Optimization*, Computational Methods in Applied Sciences 38,
DOI 10.1007/978-3-319-18320-6_15

The main burden in topology optimization is the computational cost associated with modeling the physical behavior of the optimized system. The system response is evaluated for each optimization iteration. Relatively coarse discretizations are utilized in order to save computational time. Refining the discretization improves the physical model and provides a larger solution space for the optimization process. Therefore, one of the main goals in the development of the methodology is to reduce the computational complexity without restricting the design freedom. Several approaches like material homogenization, coupled and decoupled multiscale models and efficient state solvers, discussed below, are suggested in the literature.

The systematic design of novel materials with extremal properties using topology optimization has been demonstrated in several papers starting with the pioneering work for 2D designs presented in [28, 29] to the recent manufacturable 2/3D material designs with negative Poisson's ratio [5, 35]. The optimization is performed on periodic microstructures with the aim to achieve prescribed effective properties. Such optimization affects indirectly the macroscopic response and an alternative multiscale approach to the topological design is to introduce homogenized microstructural properties in the optimization of a macrostructural response. This coincides with the original homogenization approach to topology optimization presented in [6]. The macroscale design is realized with homogenized material properties without the need to precisely specify the unit cell topology. Later a hierarchical optimization strategy has been applied to bone modeling [12, 13] where the microscopic structure and the macroscopic density are designed simultaneously. The macroscale response is decoupled from the microscale and the microstructural details affect the macroscale response through the homogenized material properties. The scale separation reduces the computational cost, however, the design often lacks connectivity between the varying microstructural details. Furthermore, practical realizations of such designs with modern manufacturable technologies (e.g. [5]) lead to finite size periodic cells, which contradict the infinite periodicity assumption applied in the homogenization process.

Here, the macroscale response of the system is completely coupled to the structural response at the microscale. The fine discretization of the physical system requires the solution of large linear systems of equations. The system response can be obtained using direct or iterative solvers. Direct solvers are often preferable due to their robust behavior, however, for large 3D problems, the computational time becomes prohibitive even on large parallel systems. On the other hand, even though they lack the robustness of direct solvers, iterative solvers provide scalable and easy to implement parallel solutions. Their convergence is improved by utilizing preconditioning techniques [26] which in the context of topology optimization are discussed in [1, 2, 4].

Here iterative solvers with preconditioning using the multiscale finite element method (MsFEM) for high-contrast media are utilized, in order to speed up the design process and to allow the optimization of large scale problems without compromising the resolution. The original MsFEM [19] represents the system behavior by constructing basis functions on a coarse grid. The coarse basis functions provide a good approximation to the system response and reduce significantly the problem

size. The method has been applied mainly to scalar problems, and recently extensions to elasticity [11] and problems modeled by positive definite bilinear forms [17], have been demonstrated as well. The MsFEM for high-contrast media [18] constructs several basis functions per coarse node, which represents well the important features of the solution with a convergence rate independent of the contrast. The method has been extended and applied to topology optimization problems in linear elasticity in [3, 22] and is presented in details in Sect. 5.

2 Physical Models

The partial differential equations (PDEs) governing the physical behavior for heat transfer and linear elasticity are introduced for 2D in the following subsections. The presented examples follow this simplification. However, the approach considered in this book chapter can be extended to 3D without any significant modifications, which will be demonstrated in following works.

2.1 Heat Transfer

The system response for heat transfer problems in a conductive medium distributed in a given domain Ω is governed by the following PDE

$$-\nabla^{\mathsf{T}}\mathbf{q} + p\,(\mathbf{x}) = 0 \quad \mathbf{x} \in \Omega \tag{1}$$

where $\mathbf{q}$ is the heat flux per unit area and $p\,(\mathbf{x})$ is a source term. The conductive heat flux $\mathbf{q}$ is obtained from Fourier's law as

$$\mathbf{q} = -\kappa \nabla\theta \tag{2}$$

where $\kappa_{\min} \leq \kappa\,(\mathbf{x}) \leq \kappa_{\max}$ is a spatially-varying conduction coefficient and θ is a scalar temperature field defined over the domain Ω. The boundary $\Gamma = \partial\Omega$ is decomposed into disjoint subsets $\Gamma = \overline{\Gamma_D \cup \Gamma_N}$. The following boundary conditions are prescribed on the different subsets

$$\theta = 0 \quad \text{on} \quad \Gamma_{\mathrm{D}} \tag{3}$$

$$q_n = g \quad \text{on} \quad \Gamma_{\mathrm{N}} \tag{4}$$

where $q_n = \mathbf{q}^{\mathsf{T}}\mathbf{n}$.

The variational formulation [9] of the above problem is to find $u \in H_0\,(\Omega)$ such that

$$a\,(u, v) = l\,(v) \quad \text{for all} \quad v \in H_0^1\,(\Omega) \tag{5}$$

where the bilinear form a and the linear functional l are defined as

$$a(u,v) = \int_{\Omega} \kappa(\mathbf{x}) \nabla u(\mathbf{x}) \nabla v(\mathbf{x}) \, \mathrm{d}\mathbf{x} \quad \text{for all} \quad u, v \in H_0^1(\Omega) \tag{6}$$

$$l(v) = \int_{\Omega} p(\mathbf{x}) v(\mathbf{x}) \, \mathrm{d}\mathbf{x} + \int_{\Gamma_N} \kappa(\mathbf{x}) g v(\mathbf{x}) \, \mathrm{d}\mathbf{x} \quad \text{for all} \quad v \in H_0^1(\Omega) \tag{7}$$

and $H_0^1(\Omega)$ is defined as

$$H_0^1(\Omega) = \left\{ v \in H^1(\Omega) : v = 0 \text{ on } \Gamma_D \right\} \tag{8}$$

$H^1(\Omega)$ is a standard Sobolev space on Ω. The Galerkin formulation of Eq. 5 is obtained using the finite element space $V_h(\Omega) \subset H_0^1(\Omega)$ with test and trial functions $u, v \in V_h(\Omega)$. The space $V_h(\Omega)$ consists of standard Lagrange shape functions defined on a uniform rectangular mesh $\mathscr{T}^h$ with characteristic length h. The Galerkin formulation leads to a linear system of equations of the form

$$\mathbf{K}\mathbf{u} = \mathbf{f} \tag{9}$$

where the vector $\mathbf{u}$ consists of all nodal values of the temperature field θ and $\mathbf{f}$ is a vector with the supplied input to the system.

2.2 Linear Elasticity

The response of a linear elastic system is governed by the Navier-Cauchy partial differential equation, e.g. [9], given as

$$\nabla \cdot \sigma(\mathbf{u}) + \mathbf{f}(\mathbf{x}) = 0, \quad \mathbf{x} \in \Omega \tag{10}$$

$$\sigma(\mathbf{u}) = \mathbf{C} : \varepsilon(\mathbf{u}) \tag{11}$$

where σ is the stress tensor, ε is the linearized strain tensor, the vector $\mathbf{u}$ consists of the displacements in the coordinate directions and $\mathbf{C}$ is the linear elastic stiffness tensor. The vector function $\mathbf{f}(\mathbf{x})$ represents the system input. The mechanical system occupies the bounded domain Ω, where the boundary $\Gamma = \overline{\Gamma_{D_i} \cup \Gamma_{N_i}}$ is decomposed into two disjoint subsets for each component $u_i, i = 1, 2$. Γ_{D_i} is the part of the boundary where $u_i = 0$ and Γ_{N_i} denotes the part with prescribed traction t_i. The stiffness tensor is isotropic with predefined Poisson's ratio $\nu < 0.5$ and spatially-varying Young's modulus $E_{\min} \leq E(\mathbf{x}) \leq E_{\max}$.

The weak formulation of the linear elasticity problem is to find $\mathbf{u} \in V_0$ such that

$$a(\mathbf{u}, \mathbf{v}) = l(\mathbf{v}) \quad \text{for all} \quad \mathbf{v} \in V_0 \tag{12}$$

with bilinear form a and linear functional l defined as

$$a(\mathbf{u}, \mathbf{v}) = \int_{\Omega} (\mathbf{C} : \varepsilon(\mathbf{u})) : \varepsilon(\mathbf{v}) \, \mathrm{d}\mathbf{x} \quad \text{for all} \quad \mathbf{v} \in V_0 \tag{13}$$

$$l(\mathbf{v}) = \int_{\Omega} \mathbf{f} \cdot \mathbf{v} \mathrm{d}\mathbf{x} + \int_{\Gamma_N} \mathbf{t} \cdot \mathbf{v} \mathrm{d}\mathbf{x} \quad \text{for all} \quad \mathbf{v} \in V_0 \tag{14}$$

where the space V_0 is defined as

$$V_0 = \left\{ \mathbf{v} \in \left[H^1(\Omega) \right]^2 : v_i = 0 \text{ on } \Gamma_{D_i}, i = 1, 2 \right\} \tag{15}$$

The weak formulation is discretized using standard finite element functions defined on uniform rectangular mesh $\mathscr{T}^h$. Similar to the heat transfer case, the discrete formulation results in a linear system of the form given by Eq. 9 with vector $\mathbf{u}$ consisting of all nodal displacements.

3 Topology Optimization Formulation

Topology optimization is an iterative method that seeks to distribute material in a given design domain by optimizing an objective functional and fulfilling a set of design constraints [7]. The material distribution is represented by a density field $0 \leq \rho(\mathbf{x}) \leq 1$. The density field takes values one for all points in the design domain Ω occupied with material and zero for the void regions. In order to utilize gradient-based optimization techniques, the density field is allowed to take intermediate values.

The main steps in the topology optimization algorithm will be demonstrated first for thermal compliance minimization, which coincides with the first example in Sect. 6. The optimization problems is defined as

$$\begin{aligned} \min_{\rho \in \mathscr{Q}_{ad}} \; & :c(\rho, u) = \int_{\Omega} \kappa(\rho(\mathbf{x})) \nabla u(\mathbf{x}) \nabla u(\mathbf{x}) \, \mathrm{d}\mathbf{x} \\ \text{s.t.} \; & a(\rho; u, v) = l(v) \\ & \int_{\Omega} \rho \mathrm{d}\mathbf{x} \leq V^* \end{aligned} \tag{16}$$

where $\mathscr{Q}_{ad}$ is the space of admissible density material distributions, V^* is the allowed volume of material and $a(\rho; u, v)$ is the bilinear from given by Eq. 6. In the optimization problem, the bilinear form Eq. 6 depends on the density field ρ. The heat conduction coefficient in Eq. 2 is interpolated between $\kappa_{\min}$ and $\kappa_{\max}$ using the modified SIMP scheme [7] given as

$$\kappa = \kappa_{\min} + (\kappa_{\max} - \kappa_{\min}) \rho^p \tag{17}$$

where p is the penalization parameter, $\kappa_{\max}$ is the conduction coefficient of the solid material, and $\kappa_{\min}$ is set to be a very small number in order to ensure that the bilinear form is coercive. The above optimization problem can be written in discrete form using the finite element discretization given by Eq. 9. The design field ρ is represented using independent design variables associated to each element. The discrete problem is given as

$$\begin{aligned} \min_{\rho} :\ & c = \mathbf{f}^{\mathsf{T}}\mathbf{u} \\ \text{s.t. } & \mathbf{K}\mathbf{u} = \mathbf{f} \\ & \rho^{\mathsf{T}}\mathbf{v} \leq V^* \\ & 0 \leq \rho_i \leq 1 \quad i = 1, \ldots, n_{\text{el}} \end{aligned} \tag{18}$$

where the vector ρ consists of all design variables and $\mathbf{v}$ is a vector with element v_i equal to the volume of the ith finite element.

The optimization problem is solved using the so-called nested formulation, where the discrete system of equations for the state problem is solved during each optimization step. The gradients of the objective with respect to the design variables are computed using adjoint sensitivity analysis [7] and are given as

$$\frac{\partial c}{\partial \rho_e} = -p\rho_e^{p-1}\left(\kappa_{\max} - \kappa_{\min}\right)\mathbf{u}_e^{\mathsf{T}}\mathbf{K}_{0,e}\mathbf{u}_e, \quad e = 1, \ldots, N_{\text{el}} \tag{19}$$

The design update is performed using the method of moving asymptotes (MMA) [31].

The optimization problem defined by Eq. 18 is mesh dependent. Instead of obtaining a better representation of a coarse optimized topology, the optimization might result in a completely different topology by refining the mesh. Such behavior is avoided here by utilizing density filtering [8, 10]. The filtered density $\rho_f(\mathbf{x})$ at a point $\mathbf{x}$ in the design domain is obtained using convolution of the original design field ρ and a filter function

$$\rho_f(\mathbf{x}) = \int_{\Omega} F(\mathbf{x} - \mathbf{y})\,\rho(\mathbf{y})\,\mathrm{d}\mathbf{y} \tag{20}$$

The filter function is chosen to be

$$F(x) = \frac{1}{R}\left(1 - \frac{|x|}{R}\right), \quad x \in [-R, R] \tag{21}$$

where R is the filter radius, which controls the length scale. Instead of using an explicit weighting function $F(\cdot)$, the filtered field can be obtained as a solution of a PDE [24] given as

$$-r^2 \triangle \rho_f + \rho_f = \rho \tag{22}$$

with $r = R/(2\sqrt{3})$. The PDE filter simplifies the enforcement of different boundary conditions on the density field, reutilizes the already developed discretization framework for solving the state problem, simplifies large scale parallel implementations of the topology optimization process, and reduces the computational cost in 3D [1, 2, 24]. The classical filter is utilized for the heat transfer example and the PDE filter is utilized for the linear elastic designs.

4 Robust Design

The filtered field consists of large gray regions which require post-processing of the optimized results. Such a transformation can affect the optimality of the solution and in many cases [34] completely destroy the performance of the optimized design. These post-processing effects are alleviated here by using projection and introducing a requirement on the performance to be insensitive with respect to uncertainties in the geometry [23, 34]. The physical density in this case is represented by a projected density field obtained as

$$\rho_p = \frac{\tanh(\beta\eta) + \tanh\left(\beta\left(\rho_f - \eta\right)\right)}{\tanh(\beta\eta) + \tanh\left(\beta\left(1 - \eta\right)\right)} \tag{23}$$

where η is a selected threshold and β controls the sharpness of the projections. For $\beta \to \infty$ the above expression approaches a Heaviside function. The gradients of the objective functional and the constraints with respect to the original design field ρ are obtained by the chain rule.

The projection improves the contrast in the design, however, the length scale imposed from the filter is lost. All manufacturing processes introduce uncertainties in the realizations of the optimized designs, which might result in complete loss of the performance [21, 34, 36]. Imperfections along the design perimeter can be modeled by varying the threshold η in Eq. 23, and for cases with non-uniform uncertainties the threshold can be replaced with spatially-varying random field [27].

Here the threshold is assumed to be a random variable with uniform distribution $\eta \in [\eta_d; \eta_e]$, where the threshold η_d corresponds to the most dilated design and η_e corresponds to the most eroded case. The optimization problem is posed as follows

$$\begin{aligned} \min_{\rho} :\ & c = \mathrm{E}\left[\mathbf{f}^{\mathsf{T}}\mathbf{u}\right] + w\sqrt{\mathrm{Var}\left[\mathbf{f}^{\mathsf{T}}\mathbf{u}\right]} \\ \text{s.t. } & \mathbf{K}\mathbf{u} = \mathbf{f} \\ & \mathrm{E}\left[\rho^{\mathsf{T}}\mathbf{v}\right] \leq V^* \\ & 0 \leq \rho_i \leq 1 \quad i = 1, \ldots, n_{\mathrm{el}} \end{aligned} \tag{24}$$

where $\mathrm{E}[\cdot]$ and $\mathrm{Var}[\cdot]$ denote the expected value and the variance of a given quantity, and w is a weight factor. The state problem in the above formulation becomes stochastic and approximations to expectation and the variance are obtained using Stochastic collocation and Monte Carlo sampling [25]. The gradients are computed as described in [23].

5 Multiscale Finite Element Method

Topology optimization is an iterative approach which requires the computation of the state solution, and possibly adjoint solution also, at every design iteration. Often, the required state and adjoint field computations account for more than 95–99 % of the total computational time [2]. The solution for small problems is usually obtained using direct solvers due to their robustness. Realistic 3D and large 2D designs with fine details require fine resolutions, which makes the computational cost prohibitive. An alternative is to use iterative solution techniques [26] also known as Krylov iterative methods. Iterative solvers alleviate some of the issues observed with direct solvers in terms of memory utilization and parallel scalability. However, their convergence speed is determined by the condition number of the system matrix, which can be improved by preconditioning.

Classical preconditioners such as incomplete factorization, diagonal scaling and successive over-relaxation, cannot provide mesh independent convergence. Furthermore, for problems with high contrast between material parameters, as the ones arising in topology optimization, the number of iterations increases with increasing contrast [2, 4]. Mesh independent convergence can be obtained using geometric multigrid (MG) [33], if the coarse grid is capable of resolving the fine scale details. Such a condition cannot be guaranteed in the topology optimization process which results in deteriorated convergence. A compelling alternative demonstrated in [15, 18, 20] is the multiscale finite element method (MsFEM) with spectral basis functions.

MsFEM with spectral bases has initially been developed for diffusion type problems [18, 20], for general bilinear forms [17], and extended later for topology optimization problems in linear elasticity [3, 22]. Here the method is presented for heat transfer problems and follows closely [18]. The idea is to construct a coarse space capable of representing the important features of the solution.

The fine mesh $\mathscr{T}^h$ utilized for the discretization of Eq. 1 and 2 is assumed to be obtained by a refinement of a coarser one $\mathscr{T}^H = \left\{K_j\right\}_{j=1}^{N_{cc}}$, where K_j denotes a coarse mesh cell and N_{cc} the number of coarse cells (e.g. Fig. 1). The nodes of the coarse mesh are denoted as $\{\mathbf{y}_i\}_{i=1}^{N_c}$, where N_c denotes the number of coarse nodes. The neighborhood of node $\mathbf{y}_i$ is defined as

$$\omega_i = \bigcup \left\{ \overline{K}_j \in \mathscr{T}^H : \mathbf{y}_i \in \overline{K}_j \right\} \tag{25}$$

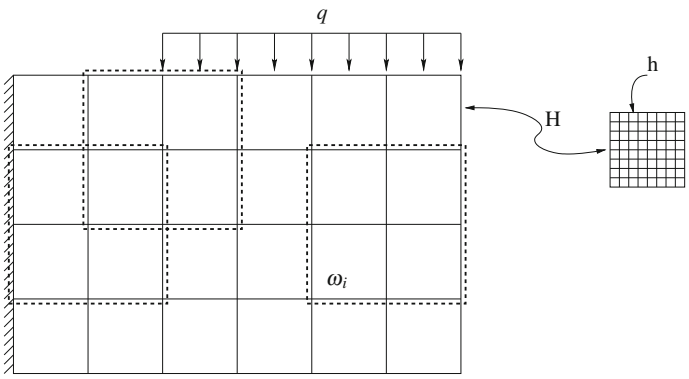

Fig. 1 Illustration of fine, coarse mesh and several agglomerates for cantilever beam subjected to distributed load q

The neighborhoods $\omega_i, i = 1, \ldots, N_c$, will be called agglomerates as they can be viewed as a group of coarse elements agglomerated together.

A set of coarse basis functions $\{\phi_{i,j},\ j = 1, \ldots, N_c\}$, defined with respect to $\mathscr{T}^h$, is introduced for each coarse node y_j. An approximation to the solution in the coarse space is sought as $u_c = \sum_{i,j} c_{i,j}\phi_{i,j}$. The coefficients $c_{i,j}$ are determined by solving the coarse problem $\mathbf{K}_c\mathbf{u}_c = \mathbf{f}_c$, with

$$\mathbf{K}_c = \mathbf{R}_c\mathbf{K}\mathbf{R}_c^{\mathsf{T}} \tag{26}$$

$$\mathbf{f}_c = \mathbf{R}_c\mathbf{f} \tag{27}$$

where $\mathbf{R}_c = \left[\phi_{i,1}, \phi_{i,2}, \ldots, \phi_{N_c,1}, \phi_{N_c,2}, \ldots\right]$ consists of all coarse basis functions defined on the fine scale grid, and $\mathbf{u}_c$ consists of all coefficients $c_{i,j}$. The matrix $\mathbf{R}_c$ provides a map between temperature fields defined on the fine and the coarse grids. An approximation to the nodal solution in the fine space can be obtained as $\mathbf{u}_a = \mathbf{R}_c^{\mathsf{T}}\mathbf{u}_c$.

The set of coarse basis functions is built using the set of eigenmodes of local eigenvalue problems [18] defined on each agglomerate ω_i. The eigenvalue problem for agglomerate ω_i is given as

$$-\nabla^{\mathsf{T}}\kappa\left(\mathbf{x}\right)\nabla u = \lambda\kappa\left(\mathbf{x}\right)u, \quad \mathbf{x} \in \omega_i \tag{28}$$

with homogeneous Neumann boundary conditions on the agglomerate boundary if $\partial\omega_i \cap \Gamma = \emptyset$, and boundary conditions applied to Eq. 1 on $\partial\omega_i \cap \Gamma \neq \emptyset$, where Γ is the boundary of the design domain Ω and $\partial\omega_i$ is the boundary of the agglomerate ω_i. The eigenvalue problem is discretized using $V_h\left(\omega_i\right) = \{v_h \in V_h :\ \text{supp}\ v_h \subset \omega_i\}$ and in matrix vector form is given as

$$\mathbf{K}_{\omega_i}\psi_j^{\omega_i} = \lambda_j^{\omega_i}\mathbf{M}_{\omega_i}\psi_j^{\omega_i} \tag{29}$$

where $\mathbf{K}_{\omega_i}$ is the stiffness matrix, $\mathbf{M}_{\omega_i}$ is a mass matrix, $\psi_j^{\omega_i}$ is the jth eigenvector, and $\lambda_j^{\omega_i}$ is the jth eigenvalue. The eigenvalues are ordered as $\lambda_1^{\omega_i} \leq \lambda_2^{\omega_i} \leq \cdots \leq \lambda_j^{\omega_i} \leq \ldots$, and the first eigenvectors corresponding to eigenvalues smaller than a selected threshold λ_Ω are selected to form the coarse basis. The coarse basis functions, represented on the fine grid, are defined as $\phi_{i,j} = \xi_i \psi_j^{\omega_i}$, i.e., they are constructed by multiplication of the eigenfunctions $\psi_j^{\omega_i}$ with a partition of unity $\{\xi_i\}_{i=1}^{N_c}$ subordinated to ω_i such that $\xi_i \in H^1(\Omega)$ and $|\nabla \xi_i| \leq 1/H, i = 1, \ldots, N_c$, where H is the characteristic length of a coarse element K. Hence, for each coarse node, the basis functions $\{\phi_{i,j}\}$ are defined as the fine space finite element interpolants of $\xi_i \psi_j^{\omega_i}$, $j = 1, \ldots, N_i$, where N_i is determined as the number of eigenvalues smaller than the globally selected threshold λ_Ω. It is important to note that, since the eigenvalue problem defined on agglomerate ω_i and the full problem share the same boundary conditions on the common boundaries, the eigenfunctions and hence the coarse basis functions automatically fulfill the boundary conditions of the global problem. The construction process of several coarse basis functions is exemplified in Fig. 2.

In [18] the coarse system is utilized as a solver, where the accuracy of the coarse approximation depends on the global threshold λ_Ω, which controls the number of the basis functions and the computational cost. For topology optimization problems

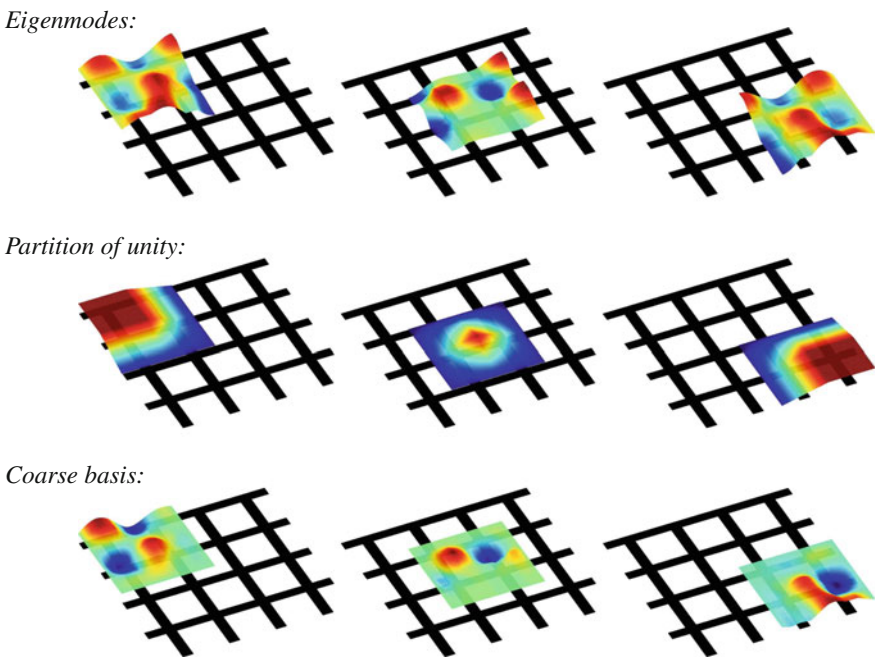

Fig. 2 Illustration of spectral basis construction

using the nested formulation, the optimizer can take advantage of the approximation error. As discussed in [22], the optimization for linear elasticity might result in isolated islands of material. Such topologies are not optimal and appear due to the homogenization effect of the approximation. Therefore, here the coarse solver is utilized as a preconditioner for iterative solvers applied to the fine-scale problem. Using the coarse system as a preconditioner results in mesh- and contrast-independent number of iterations for the Preconditioned Conjugate Gradient (PCG) and the Generalized Minimal Residual Method (GMRES). In [20] the coarse space is utilized in a two-level additive Schwarz preconditioner. Instead of implementing local subdomain solvers for the Schwarz preconditioner, here, the coarse space is utilized as a coarse-level in a two-level multigrid preconditioner for GMRES (e.g. [33]). The smoothing is performed by a single symmetric Gauss-Seidel step.

The time consuming part of the MsFEM algorithm is the construction of the coarse basis and the projection given by Eq. 26. Several strategies for reducing the computational cost are discussed in [3, 22]. The main idea utilizes the fact that the design changes during the optimization process are relatively slow and hence consecutive design realizations can share the same coarse basis. When the difference in the topologies for the reference and the current design becomes large, the basis is updated. A heuristic rule is suggested in [3] where the basis is updated when the solver iterations exceed the previous iteration number by more than a given limit. More rigorous criteria is a subject of future research. In the stochastic case, the basis is constructed for the most dilated design and utilized for all realizations which further reduces the computational cost. For linear elastic problems, the MsFEM coarse basis algorithm follows the same steps and is demonstrated in [3, 22].

6 Numerical Examples

6.1 Heat Sink Design

The first example is the topology optimization of thermal compliance. The design domain is shown in Fig. 3. The temperature T_0 is set to zero. The conduction coefficient of the solid material is set to one and the conduction of the void region is 10^{-6}. The volume occupied with solid material is restricted to be 50 % of the total volume. Uniform heat flux is supplied over the design domain. The penalization factor p is increased from 1.2 to 3.0 after the first 100 iterations. The projection coefficient β is increased from 8 to 32 after the first 200 iterations. The optimization is performed with three realizations $\eta_e = 0.7$, $\eta_i = 0.5$ and $\eta_d = 0.3$ of the threshold projection $\eta \in [0.3, 0.7]$ and are verified by Monte Carlo simulations. Four coarse cell configurations with 4×4, 8×8, 16×16 and 32×32 coarse cells, are selected. Each coarse cell consists of 40×40 elements. The filtering step is performed with standard hat filter function with radius $R = 3\,\mathrm{h}$. All coarse cells are kept identical. The optimization problem in discrete form is given by Eq. 24 with $w = 1$.

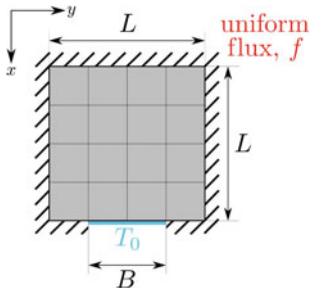

Fig. 3 Heat sink optimization problem—design domain with dimensions L and $B = L/2$. Unit heat flux is applied uniformly over the design domain

Fig. 4 Optimized heat sink topology for 4×4, 8×8, 16×16 coarse cells

Fig. 5 Optimized heat sink coarse cell topology for 4×4, 8×8, 16×16 and 32×32 coarse cells

Optimized topologies for the heat sink design problem are shown in Fig. 4 and enlarged cell designs are shown in Fig. 5. The mean objective values for the four considered cases are 46.3; 12.8; 7.3; 3.7. The decrease in the compliance is due to the nature of the problem. The optimal design will consists of smaller and smaller features covering more uniformly the design domain due to the distributed flux. Increasing the number of coarse cells with a constant relative length scale at the microscale, results in a smaller overall design length scale which improves the objective. The length scale is imposed with respect to the cell characteristic length and is not related to the global macroscale. It can be observed that the cell topology is not preserved during

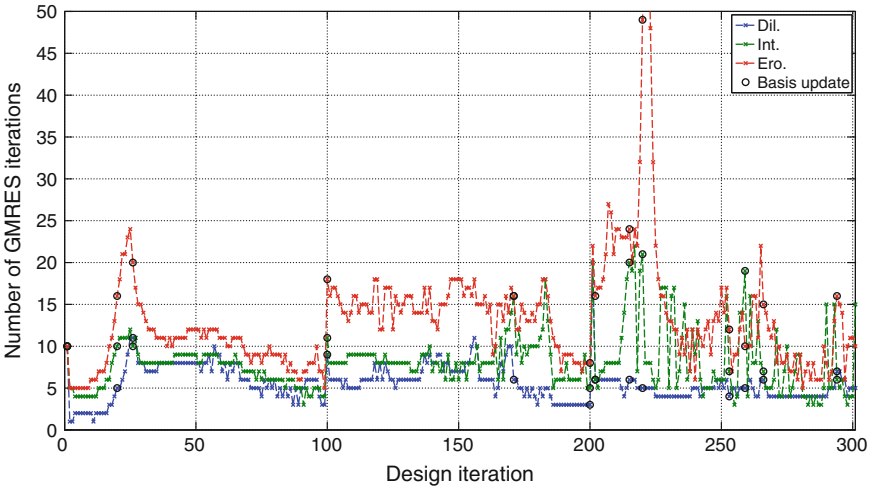

Fig. 6 GMRES iterations for relative tolerance 10^{-5}. The circles denote the basis updates

the refinement. The GMRES iteration number is kept under 20 with the selected eigenvalue threshold. Increasing the threshold, decreases the iteration number. However, as the cost for computing the basis increases, it also results in an increase of the total computational time [3]. The basis is obtained for the dilated realization, and thus the GMRES iterations differ between the realizations, as seen in Fig. 6. An alternative is the reduced basis approach as suggested in [16], which provides good coarse space for all realizations. However, this increases the computational cost related to the eigenproblems and results in longer optimization time.

The selection of the eigenvalue threshold is a non-trivial task and needs further investigations. The value and the computational time depend on the CPU architecture, the implementation of the preconditioner, the eigenvalue solver and the number of unique agglomerates in the design. For the selected example only ten unique agglomerates can be identified. As demonstrated in [22], MsFEM can also be applied to general problems without microstructure. Such an approach removes the restrictions on the design space and the design performance is expected to improve further. However, the design freedom comes at higher computational cost due to the large number of local eigenvalue problems. All of them are completely independent. Thus, the MsFEM preconditioner will excel in parallel implementations which are subject to future research. It should be noted that for the small 2D problems, the total computational time becomes larger compared to the total time with direct solvers. However, increasing the problems size leads to shorter computational times for the proposed approach [3].

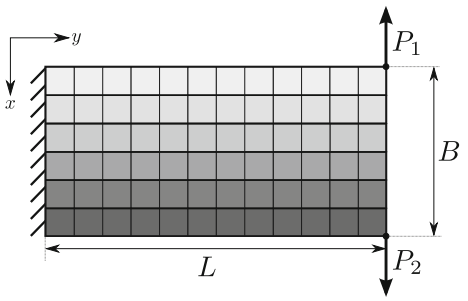

Fig. 7 Boundary conditions and design domain of layered cantilever beam problem with multiple load cases. The *vertical* dimension is $B = L/2$

6.2 Linear Elastic Designs with Multiple Load Cases

The second example, shown in Fig. 7, is the design of a cantilever beam with two load cases. For the first load case the only active force is P_1 and for the second case P_2. The coarse mesh consists of 16×8 coarse cells and periodicity is enforced only in the horizontal direction. The filtering step is performed using the PDE filter with filter parameter $R = 4\,\mathrm{h}$, where h is the characteristic length of the fine mesh. Each coarse cell consists of 40×40 elements. The weight coefficient in the stochastic formulation is set to 1.0. The volume fraction is 30 % of the design domain volume. The Poisson's ratio is set to $\nu = 0.3$, the modulus of elasticity for the solid is set to $E_{\max} = 1$, and the modulus of elasticity for the void material is set to $E_{\min} = 10^{-9}$. The rest of the parameters are set to be the same as for the thermal case, except that the final value of p is set to 5.0. The optimization problem is given as

$$\begin{aligned} \min_{\rho} :\ & c = \sum_{i=1}^{n_l} \mathrm{E}\left[\mathbf{f}_i^{\mathsf{T}}\mathbf{u}_i\right] + w\sqrt{\mathrm{Var}\left[\mathbf{f}_i^{\mathsf{T}}\mathbf{u}_i\right]} \\ \text{s.t. } & \mathbf{K}\mathbf{u}_i = \mathbf{f}_i, \quad i = 1, \ldots, n_l \\ & \mathrm{E}\left[\rho^{\mathsf{T}}\mathbf{v}\right] \leq V^* \\ & 0 \leq \rho_i \leq 1 \quad i = 1, \ldots, n_{\mathrm{el}} \end{aligned} \tag{30}$$

where n_l is the number of load cases.

The optimized design is shown in Fig. 8. In contrast to the designs obtained for a single active load presented in [3], the obtained design is symmetric with respect to the horizontal mid-axis and the microstructural details closely resembles triangular truss structures. Triangular truss-like structures are optimal for problems with changes of the principal stress orientation for the different load cases. For a single load case without any restrictions on the design pattern, the optimal design will follow the principal stress trajectories. The mean compliance is 2.9 for both load cases. Optimization for a single load case resulted in a mean compliance of 2.5 which as expected is better for that particular load case, and worse for the load in the other direction yielding a compliance of 3.8.

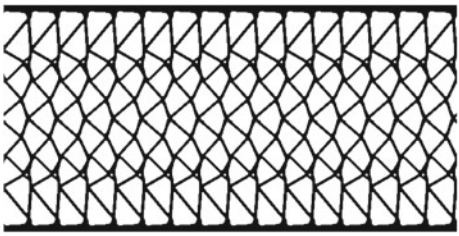

Fig. 8 Intermediate design realization $\eta = 0.5$ for optimized multiple load cases cantilever beam problem

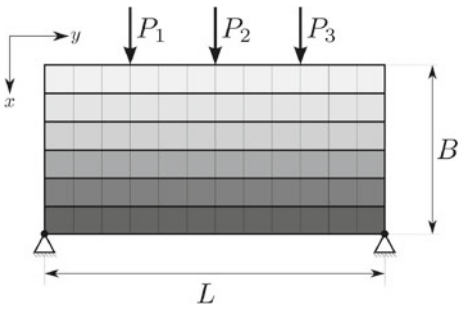

Fig. 9 Boundary conditions and design domain of layered beam problem with multiple load cases

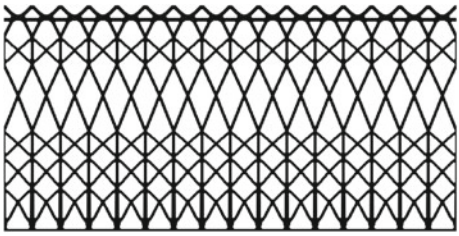

Fig. 10 Intermediate design realization $\eta = 0.5$ for optimized multiple load case beam problem

The third example, shown in Fig. 9, is the design of a simply supported beam with three load cases. The optimization setup parameters are the same as for the previous example. The optimized intermediate design realization is shown in Fig. 10. The multiload case design shares some similarities to the single load case with central active force $P_2 = 1$ shown in Fig. 11. However, a cross-check of the designs show that it performs better for all three cases in contrast to the single load designs which perform well only for the corresponding design case. Requiring periodicity in the horizontal direction implicitly ensures some robustness of the P_2 single load case with respect to a shift of the applied load with a single or multiple coarse cells. This property is not shared for the single load designs obtained for P_1 or P_3. The microstructural details vary along in the vertical direction, however, some of the layers show similar topology with small variations.

The periodicity requirement implicitly imposes a maximum length scale on the design [3] as it requires the material to be distributed regularly along the design domain. Removing the periodicity requirement in the horizontal direction would provide additional freedom to the optimizer and would allow more material to be

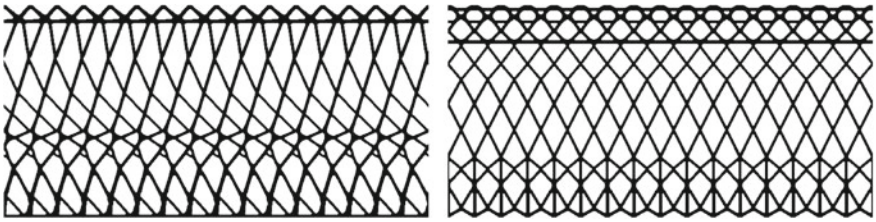

Fig. 11 Intermediate design realization $\eta = 0.5$ for optimized single load case beam problems—P_1 is active on the first design (*left*) and P_2 is active on the second design (*right*)

concentrated in the central areas of the beam, which will result in better performance. Therefore, such restrictions on the design space should be imposed only for manufacturing, aesthetic or other reasons not related directly to the optimality of the design. As mentioned earlier, the computational cost of the coarse basis increases with increasing the design freedom. However, for multiple load cases the basis is utilized for multiple solutions which makes the approach even more competitive compared to the alternatives.

6.3 Linear Elastic Designs with Zero and Negative Expansion

The final example is topology optimization of a linear elastic compression test with restrictions on the horizontal displacements. The boundary conditions and the design domains are shown in Fig. 12. Two cases are considered: for the first, a solid region of thickness $t = 0.0125$ is enforced only on the top of the design domain, and for the second, the solid region is enforced on the horizontal edges as well. The design domain is partitioned using 8×8 coarse cells with design symmetry with respect to the vertical axis. Each coarse cell is discretized using 40×40 finite elements. The filtering is performed by the PDE filter with parameter $R = 5\,\mathrm{h}$. The dilated, intermediate and eroded design thresholds are set to 0.4, 0.5 and 0.6, respectively.

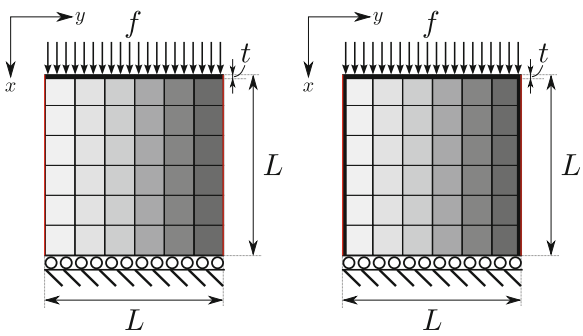

Fig. 12 Boundary conditions and design domains for compression tests with restrictions on the horizontal displacements. *Solid regions* marked with *thick black line* are enforced on the *top edge* in the first case (*left*) and also on the *horizontal edges* in the second case (*right*)

The dimension of the design domain is set to $L = 2$. Distributed load of total size 10^{-3} is applied on the upper edge of the design for the two cases. The material volume is restricted to be 50 % of the design domain volume. The penalization is set to $p = 5$ and the projection parameter β is increased from 8 to 32 after the first 150 iterations. The rest of the optimization parameters are the same as for the previous example.

The optimization formulation in discrete form is given as

$$\begin{aligned} \min_{\rho} : \quad & c = \mathrm{E}\left[\mathbf{f}^{\mathsf{T}}\mathbf{u}\right] + w\sqrt{\mathrm{Var}\left[\mathbf{f}^{\mathsf{T}}\mathbf{u}\right]} \\ \text{s.t.} \quad & \mathbf{K}\mathbf{u} = \mathbf{f} \\ & \mathrm{E}\left[\rho^{\mathsf{T}}\mathbf{v}\right] \leq V^* \\ & \bar{\mathbf{u}}_j + \sigma_j - u_{\mathrm{ref}} \leq \varepsilon_{con},\ j = e, i, d \\ & \bar{\mathbf{u}}_j - \sigma_j - u_{\mathrm{ref}} \geq \varepsilon_{con},\ j = e, i, d \\ & 0 \leq \rho_i \leq 1 \quad i = 1, \ldots, n_{\mathrm{el}} \end{aligned} \tag{31}$$

where the expectation and the variance in the objective are approximated using only three realizations: the most eroded case $\eta_e = 0.6$, the most dilated case $\eta_d = 0.4$ and the intermediate case for $\eta_i = 0.5$. The final results are verified using Monte Carlo simulations. The objective is to minimize the compliance of the system with constraints on the horizontal displacements along the vertical edges, where $\bar{u}_j$, $j = e, i, d$, is the average displacement along the horizontal edge for the eroded, intermediate and dilated realizations, respectively, σ_j is the standard deviation of the horizontal displacements along the edge for realization j, and ε_{con} is a prescribed tolerance.

The initial design is obtained by repetition of a unit cell negative Poisson's ratio design from [35]. The unit cell design is robust with respect to uniform erosion and dilation. Deformed structures for the considered cases are shown in Fig. 13. The global behavior of the two structures differs significantly due to the difference in the boundaries. For the first case of unframed design, the bulk material is free to contract and the negative Poisson's effect can be clearly seen. In the second case, the stiff frame around the bulk material restrains the horizontal movement which lowers the Poisson's effect and adds additional stiffness to the structure in the vertical direction. This results in lower vertical displacements of the upper edge. The displacements along the vertical edge for framed and unframed designs are shown in Figs. 14 and 15. For the unframed design, the horizontal displacements for the three realizations are large and negative as expected from the homogenized material properties. However, for the framed design, shown in Fig. 15, the horizontal displacements for the eroded and dilated cases are significantly smaller.

As demonstrated above, optimized microstructure designs for a selected material property might lead to different global responses for equivalent load patterns due to small differences in cells close to boundaries of the design. Classical homogenization theory [32] does not take into account the boundary conditions and localized effects.

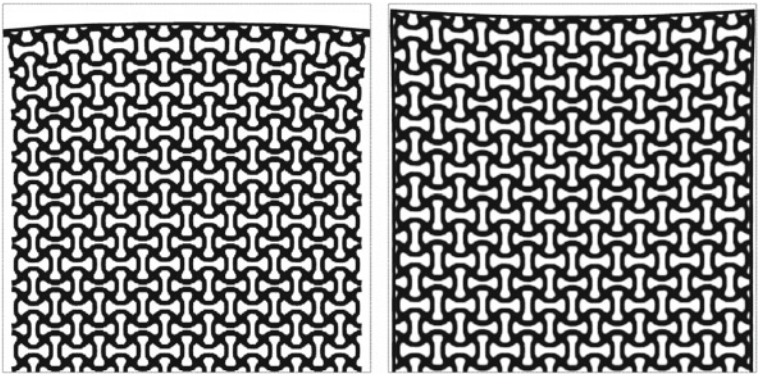

Fig. 13 Deformed structures for unframed (*left*) and boxed (*right*) design domains with microstructural pattern optimized for negative Poisson's ratio

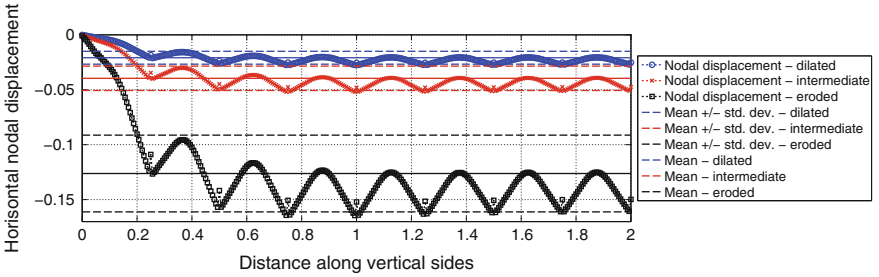

Fig. 14 Horizontal displacements along the *vertical edge* of the design domain with unframed boundaries for design realizations with thresholds 0.4, 0.5 and 0.6 (dilated, intermediate, and eroded)

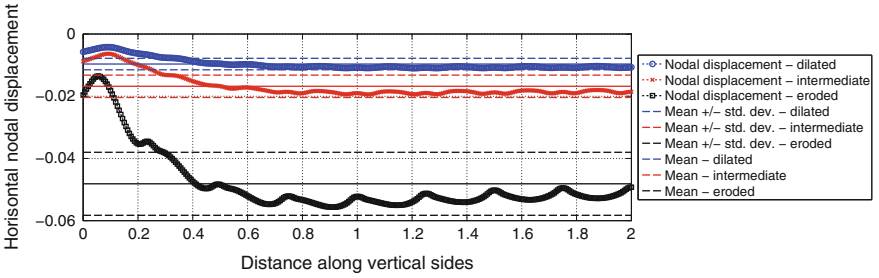

Fig. 15 Horizontal displacements along the *vertical edge* of the design domain with framed boundaries for design realizations with thresholds 0.4, 0.5 and 0.6 (dilated, intermediate, and eroded)

Hence, in all cases where the global structural response is of interest, the boundary effects should be taken into account during the optimization process. As demonstrated here, the proposed MsFEM methodology provides such solution at a relatively low computational cost.

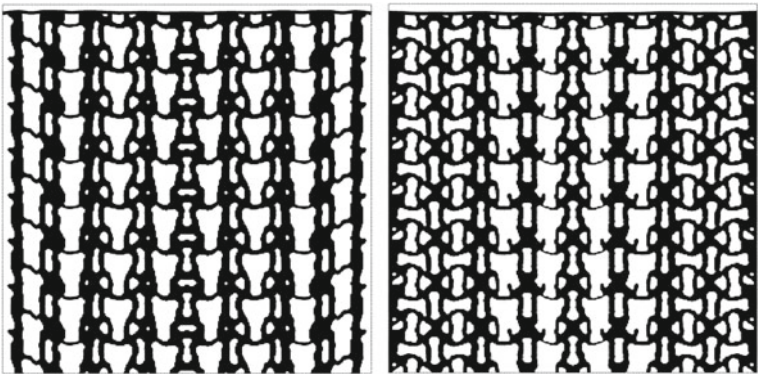

Fig. 16 Deformed structures for unframed (*left*) and framed (*right*) design domains with microstructural patterns optimized for tailoring macroscale response. The reference horizontal displacement along the *vertical edge* is zero

Topology optimized design, using the formulation given by Eq. 31, with zero reference displacement $u_{\text{ref}} = 0$ and $\varepsilon_{\text{con}} = 10^{-4}$, are shown in Fig. 16. The microstructures differs significantly close to the vertical edges, which demonstrates the need to account for boundary effects in the design process. In the first case, the optimization utilizes the fact that solid material is not required along the vertical edge and shifts the force transmitting structure from the boundary. In the second case, a complex microstructure is designed around the solid frame in order to avoid displacements in the horizontal direction. Another important feature observed during the design process, is that the eroded, dilated and intermediate designs might not share the same topology. In such cases length scale cannot be guaranteed on the intermedi-

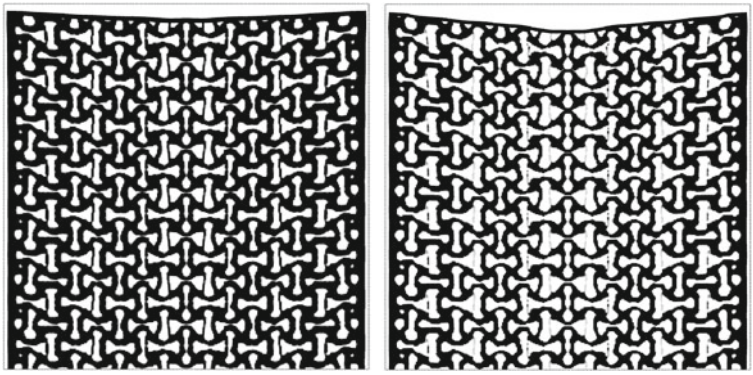

Fig. 17 Dilated (*left*) and intermediate (*right*) deformed structures realizations for framed design domain with microstructural patterns optimized for tailoring macroscale response. The reference horizontal displacement along the vertical edge is $u_{\text{ref}} = -0.01$ and $\varepsilon_{\text{con}} = 10^{-3}$

ate design [34], however, since the design performance is insensitive with respect to small imperfections, removing or adding small features along the perimeter will not change significantly the optimized performance. This property can be clearly observed for the case with negative reference displacement shown in Fig. 17.

7 Conclusions

In this book chapter, a methodology has been demonstrated for tailoring macroscale responses of mechanical and heat transfer systems by topology optimization of microstructural details. These details are herein restricted to full periodicity or grading in a single direction. For a heat transfer problem, increased periodicity is shown to aid the optimization objective, and for certain elastic structures with multiple load cases it is shown that partial periodicity can provide an implicit robustness to load position. Finally, it has been demonstrated that it is important to take the boundary effects and finite size microstructural details into account during the optimization process in order to tailor the macroscopic response. These details can be easily accounted for by the proposed multiscale approach. The spectral MsFEM for high-contrast problems reduces the computational cost and allows for the optimization of large resolution models within a reasonable amount of time.

Acknowledgments Both authors were funded by Villum Fonden through the NextTop project, as well as the EU FP7-MC-IAPP programme LaScISO. The authors would like to thank Dr. Fengwen Wang for providing them with optimized periodic microstructural design of negative Poisson's ratio material utilized as initial guess in the last example.

References

1. Aage N, Andreassen E, Lazarov BS (2014) Topology optimization using PETSc: an easy-to-use, fully parallel, open source topology optimization framework. Struct Multi Optim 1–8. doi:10.1007/s00158-014-1157-0
2. Aage N, Lazarov B (2013) Parallel framework for topology optimization using the method of moving asymptotes. Struct Multi Optim 47(4):493–505. doi:10.1007/s00158-012-0869-2
3. Alexandersen J, Lazarov BS (2015) Topology optimisation of manufacturable microstructural details without length scale separation using a spectral coarse basis preconditioner. Comput Methods Appl Mech Eng 290(1):156–182. doi:10.1016/j.cma.2015.02.028
4. Amir O, Aage N, Lazarov BS (2014) On multigrid-CG for efficient topology optimization. Struct Multi Optim 49(5):815–829 (2014). doi:10.1007/s00158-013-1015-5
5. Andreassen E, Lazarov BS, Sigmund O (2014) Design of manufacturable 3d extremal elastic microstructure. Mech Mater 69(1):1–10. doi:10.1016/j.mechmat.2013.09.018
6. Bendsøe MP, Kikuchi N (1988) Generating optimal topologies in structural design using a homogenization method. Comput Methods Appl Mech Eng 71(2):197–224. doi:10.1016/0045-7825(88)90086-2
7. Bendsoe MP, Sigmund O (2003) Topology optimization—Theory, methods and applications. Springer, Berlin

8. Bourdin B (2001) Filters in topology optimization. Int J Numer Methods Eng 50:2143–2158
9. Braess D (2007) Finite elements: theory, fast solvers, and applications in solid mechanics. Cambridge University Press, Cambridge
10. Bruns TE, Tortorelli DA (2001) Topology optimization of non-linear elastic structures and compliant mechanisms. Comput Methods Appl Mech Eng 190:3443–3459
11. Buck M, Iliev O, Andrä H (2013) Multiscale finite element coarse spaces for the application to linear elasticity. Central European Journal of Mathematics 11(4):680–701. doi:10.2478/s11533-012-0166-8
12. Coelho P, Fernandes P, Guedes J, Rodrigues H (2008) A hierarchical model for concurrent material and topology optimisation of three-dimensional structures. Struct Multi Optim 35:107–115. doi:10.1007/s00158-007-0141-3
13. Coelho P, Fernandes P, Rodrigues H, Cardoso J, Guedes J (2009) Numerical modeling of bone tissue adaptationa hierarchical approach for bone apparent density and trabecular structure. J Biomech 42(7):830–837. doi:10.1016/j.jbiomech.2009.01.020
14. Deaton J, Grandhi R (2014) A survey of structural and multidisciplinary continuum topology optimization: post 2000. Struct Multi Optim 49(1):1–38. doi:10.1007/s00158-013-0956-z
15. Efendiev Y, Galvis J (2011) A domain decomposition preconditioner for multiscale high-contrast problems. In: Huang Y, Kornhuber R, Widlund O, Xu J, Barth TJ, Griebel M, Keyes DE, Nieminen RM, Roose D, Schlick T (eds) Domain decomposition methods in science and engineering XIX, lecture notes in computational science and engineering. Springer, Berlin, pp 189–196. doi:10.1007/978-3-642-11304-820
16. Efendiev Y, Galvis J, Hou TY (2013) Generalized multiscale finite element methods (gmsfem). J Comput Phys 251(0):116–135. doi:10.1016/j.jcp.2013.04.045
17. Efendiev Y, Galvis J, Lazarov R, Willems J (2012) Robust domain decomposition preconditioners for abstract symmetric positive definite bilinear forms. ESAIM: Math Model Numer Anal 46:1175–1199
18. Efendiev Y, Galvis J, Wu XH (2011) Multiscale finite element methods for high-contrast problems using local spectral basis functions. J Comput Phys 230(4):937–955. doi:10.1016/j.jcp.2010.09.026
19. Efendiev Y, Hou TY (2009) Multiscale finite element methods: theory and applications. Springer, Berlin
20. Galvis J, Efendiev Y (2010) Domain decomposition preconditioners for multiscale flows in high-contrast media. Multiscale Model Simul 8(4):1461–1483. doi:10.1137/090751190
21. Jansen M, Lazarov B, Schevenels M, Sigmund O (2013) On the similarities between micro/nano lithography and topology optimization projection methods. Struct Multi Optim 48(4):717–730. doi:10.1007/s00158-013-0941-6
22. Lazarov B (2014) Topology optimization using multiscale finite element method for high-contrast media In: Lirkov I, Margenov S, Waniewski J (eds) Large-scale scientific computing, lecture notes in computer science, pp 339–346. Springer, Berlin. doi:10.1007/978-3-662-43880-038
23. Lazarov BS, Schevenels M, Sigmund O (2012) Topology optimization considering material and geometric uncertainties using stochastic collocation methods. Struct Multi Optim 46:597–612. doi:10.1007/s00158-012-0791-7
24. Lazarov BS, Sigmund O (2011) Filters in topology optimization based on Helmholtz-type differential equations. Int J Numer Meth Eng 86(6):765–781. doi:10.1002/nme.3072
25. Maitre OPL, Knio OM (2010) Spectral Methods for uncertainty quantification: with applications to computational fluid dynamics. Springer, Berlin
26. Saad Y (2003) Iterative methods for sparse linear systems. SIAM, Philadelphia
27. Schevenels M, Lazarov B, Sigmund O (2011) Robust topology optimization accounting for spatially varying manufacturing errors. Comput Meth Appl Mech Eng 200(49–52):3613–3627. doi:10.1016/j.cma.2011.08.006
28. Sigmund O (1994) Materials with prescribed constitutive parameters: an inverse homogenization problem. Int J Sol Struct 31(17):2313–2329. doi:10.1016/0020-7683(94)90154-6

29. Sigmund O (1995) Tailoring materials with prescribed elastic properties. Mech Mater 20(4):351–368). doi:10.1016/0167-6636(94)00069-7
30. Sigmund O, Maute K (2013) Topology optimization approaches. Struct Multi Optim 48(6):1031–1055. doi:10.1007/s00158-013-0978-6
31. Svanberg K (1987) The method of moving asymptotes - a new method for structural optimization. Int J Numer Meth Eng 24:359–373
32. Torquato S (2002) Random heterogeneous materials. Springer, Berlin
33. Vassilevski PS (2008) Multilevel block factorization preconditioners: matrix-based analysis and algorithms for solving finite element equations. Springer, New York
34. Wang F, Lazarov B, Sigmund O (2011) On projection methods, convergence and robust formulations in topology optimization. Struct Multidi Optim 43(6):767–784. doi:10.1007/s00158-010-0602-y
35. Wang F, Sigmund O, Jensen JS (2014) Design of materials with prescribed nonlinear properties. J Mech Phys Sol 69(1):156–174. doi:10.1016/j.jmps.2014.05.003
36. Zhou M, Lazarov BS, Sigmund O (2014) Topology optimization for optical projection lithography with manufacturing uncertainties. Appl Opt 53(12):2720–2729. doi:10.1364/AO.53.002720